JOURNAL OF AIRCRAFT
Vol. 48, No. 4, July–August 2011

Design, Optimization, and Evaluation of Integrally Stiffened Al-7050 Panel with Curved Stiffeners

Wesley C. H. Slemp*
Virginia Polytechnic Institute and State University, Blacksburg, Virginia 24061
R. Keith Bird†
NASA Langley Research Center, Hampton, Virginia 23681
Rakesh K. Kapania‡
Virginia Polytechnic Institute and State University, Blacksburg, Virginia 24061
and
David Havens,§ Ashley Norris,¶ and Robert Olliffe§
Lockheed Martin Aeronautics Company, Marietta, Georgia 30063

DOI: 10.2514/1.C031118

A curvilinear stiffened panel was designed, manufactured, and tested at NASA Langley Research Center in the combined load test fixture. The panel was optimized for minimum mass subjected to constraints on buckling load, yielding, and crippling or local stiffener failure, using a new analysis tool named EBF3PanelOpt. The panel was designed for a combined compression-shear loading configuration, which is a realistic load case for a typical aircraft wing panel. The panel was loaded beyond buckling and strains, and out-of-plane displacements were extracted from a total of 32 strain gages and 5 linear variable displacement transducers. A digital photogrammetic system was used to obtain full-field displacements/strains in the lower half of the stiffened side of the panel. The experimental data were compared with the strains and out-of-plane deflections from a high-fidelity nonlinear finite element analysis. The experimental data were also compared with linear elastic finite element results of the panel/test fixture assembly. The numerical results indicated that the panel buckled at the linearly elastic buckling eigenvalue predicted by the panel/test fixture assembly. The out-of-plane displacement measured by the digital photogrammetic system compared well both qualitatively and quantitatively with the nonlinear finite element solution in the postbuckling regime. Furthermore, the experimental strains compared well with both the linear and nonlinear finite element model before buckling. For the postbuckling regime, the nonlinear model compared well at some locations and poorly at others.

Nomenclature

b	=	stiffener height, in.
E	=	Young's modulus, psi
F_{cc}	=	allowable crippling stress, psi
t	=	stiffener thickness, in.
x, y, z	=	rectilinear coordinate basis
ε	=	strain
λ_0	=	buckling eigenvalue
ν	=	Poisson's ratio
σ_{stiff}	=	minimum principle stress in the stiffener, psi
σ_{vm}	=	von Mises stress, psi
σ_y	=	yield stress, psi

I. Introduction

TOPOLOGY optimization methods for continuum structures have increased in popularity in recent years. With these methods, both two- and three-dimensional optimal solid designs can be obtained without the traditional trial and error decision making process that design engineers have used for decades. Bendsoe and Kikuchi developed the theoretical foundation for the topology optimization methodology in 1988 [1]. The first commercial software, Altair OptiStruct [2], was developed and released in 1994 and used the topology optimization approach.

A critical limitation of the topology optimization approach is its computational intensity. The density method uses the density of each element as the design variable [3]. Thus, the method can be impractical for everyday design. Furthermore, the manufacturability of the optimal design is not guaranteed. The design engineer must transfer the optimal design solution to a practical solution. In addition, difficulties arise when imposing constraints on buckling [4]. The problem arises from numerical difficulties in the presence of low material density. To overcome this difficulty, Schramm et al. [4] proposed a two-step optimization, using topology optimization to minimize compliance while placing a constraint on mass. In the second step, a size optimization was performed on the resulting topology.

Stiffened plate or shell structures are widely used in the aerospace, automobile, and ship industries. Optimization of isogrid-stiffened panels and shells has been performed for many years. Bushnell developed a software tool (PANDA2), to obtain minimum weight designs for metallic or composite panels with isogrid stiffeners subjected to buckling constraints [5]. Optimization of the size and placement of isogrids of straight stiffeners for buckling load and natural frequency was studied by Akl et al. [6]. Because the geometry is mostly defined a priori, the number of design variables is small relative to topology optimization. Traditional aircraft structures have straight stiffening members, like spars, ribs, stringers, longerons, and stiffeners of uniform thicknesses, which are riveted to fuselage/wing panels using a traditional manufacturing process. However, recent

Received 26 May 2010; revision received 18 December 2010; accepted for publication 20 December 2010.

*Graduate Research Assistant, Aerospace and Ocean Engineering, 215 Randolph Hall. Student Member AIAA.
†Materials Research Engineer, Advanced Materials and Processing Branch, Mail Stop 188A.
‡Mitchell Professor, Aerospace and Ocean Engineering. Associate Fellow AIAA.
§Aeronautical Engineer, Staff, Advanced Development Programs.
¶Material Engineer, Advanced Development Programs.

new metallic manufacturing processes, such as friction stir welding [7] and electron beam freeform fabrication (EBF3) [8], allow the design engineer to consider a more broad design space. Moreover, the topology optimization method often results in curved geometries (e.g., the fillet problem in [1]). Therefore, considering a design space in which stiffeners can take a curvilinear profile, rather than linear, may result in a reduction in mass for the same structural design requirements.

The benefits of unitized structures [9] can be summarized as follows: a) reduced part count, manufacturing cycle time, and fabrication cost; b) added design flexibility, weight savings, inspectability, and resistance to fatigue and corrosion; c) enhanced automation, improved ergonomics, and reduced work; and d) increased determinant assembly opportunities, improved fit, and reduced rework. Experts also pointed out that the use of unitized structure is expected to grow exponentially by the year 2020 [10]. Boeing [11] developed an integrally stiffened fuselage concept, for which analysis and experimental tests demonstrated equal or better performance compared with conventional designs, with regard to weight and structural integrity, while achieving a significant reduction in manufacturing cost.

A new analysis tool, EBF3PanelOpt [12–15], is being developed for design and optimization of complex multifunctional aircraft structural concepts, with application toward pressurized noncircular fuselage structures within hybrid wing/body vehicles in which complex structural load cases are not well characterized using current design databases. EBF3PanelOpt is a tool for optimization of stiffened plate and shell structures in which stiffeners are not limited by traditional manufacturing techniques. Using curved stiffeners broadens the design space without substantially adding to the computational cost of the optimization. Whereas the tool is much more computationally efficient than topology optimization techniques, in that there are very few design variables, the design space is much larger than traditional techniques that rely on linear stiffener grids. EBF3PanelOpt is being developed to exploit emerging additive manufacturing processes that offer the ability to efficiently fabricate complex structural configurations. The ultimate goal is to enhance aircraft performance and environmental responsibility, through reductions in weight, emissions, and cabin noise, and to integrate functions such as acoustic damping, adaptive active aerodynamic controls, and aeroelastically tailored structures.

The tool development is being conducted under a NASA research announcement (NRA) contract at Virginia Polytechnic Institute and State University, with support and aircraft manufacturing expertise provided through a subcontract with Lockheed Martin Aeronautics Co. The work is complementary to EBF3 additive manufacturing research activities at NASA Langley Research Center.

This paper describes the initial phases of development of the EBF3PanelOpt tool. The tool was used to design and optimize a baseline structural panel with curved stiffeners. In the case of this baseline panel, the optimization was based on minimum mass subjected to constraints on buckling load, yielding, and crippling or local stiffener failure under a combination of compression and shear loads, to evaluate the capability of the tool to handle complex loading conditions. The optimized panel design was used to fabricate an integrally machined test panel, using aluminum alloy 7075-T851. The panel was tested in the NASA Langley Research Center combined loads test fixture (CLTF) [16], under a combined compression-shear loading case. The test results were compared against a linear finite element analysis (FEA) of the test fixture/panel assembly, through which EBF3PanelOpt obtained the optimization constraints and a conventional high-fidelity nonlinear FEA. The test results and analyses were used to assess the strengths and weaknesses of the EBF3PanelOpt tool, for the next iteration of its development as a tool for structural panel design and optimization.

II. EBF3PanelOpt Framework

A framework has been developed, by researchers at Virginia Polytechnic Institute and State University, for design optimization of curvilinear stiffened panels under in-plane and transverse loading [12–15]. The framework, named EBF3PanelOpt, is an object-oriented script written in PYTHON that interfaces with MSC.Patran and MSC.Nastran to perform FEA on a panel with curvilinear, blade-type stiffeners and returns the mass of the panel and constraints on yielding, buckling, and crippling or local failure of the panel.

The EBF3PanelOpt script obtains design data from an optimizer software, such as VisualDoc, DAKOTA, or MAMOP, and translates the design data into an MSC.Patran session (.ses) file, which generates the appropriate parameterized geometry, the FE mesh (.bdf file), and an input file (.dat) to MSC.Nastran. A schematic of the EBF3PanelOpt framework may be seen in Fig. 1. The script calls Nastran to perform the FEA and waits for the analysis to complete. After completion of the FEA, the script reads the results from the .f06 file and calculates the responses. The responses include the mass, the buckling constraint, von Mises stress constraint, and the local crippling constraint. The buckling constraint is calculated by

$$\frac{1}{\lambda_0} \leq 1 \tag{1}$$

where λ_0 is the buckling eigenvalue. The von Mises stress constraint is calculated by

$$\frac{\sigma_{\text{vm}}}{\sigma_y} \leq 1 \tag{2}$$

where σ_{vm} is the von Mises stress, and σ_y is the material yield strength. The von Mises stress constraint is imposed using the Kreisselmeir–Steinhauser criteria for constraint aggregation, as described in [2]. The crippling constraint was calculated by

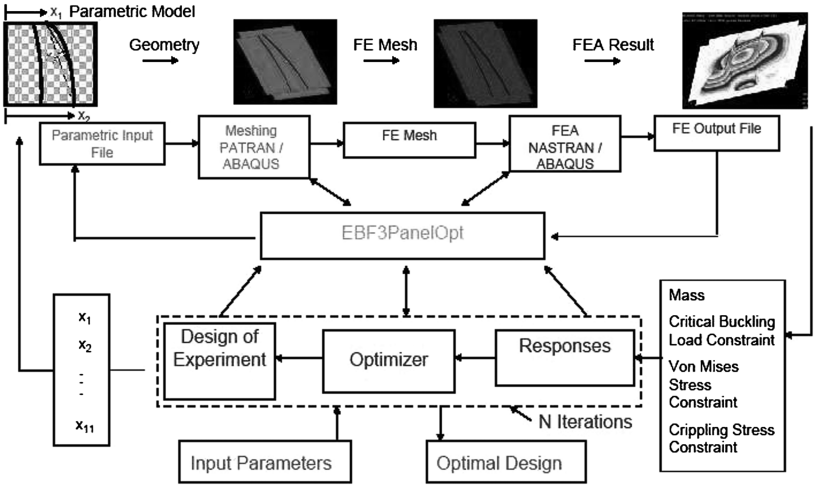

Fig. 1 Schematic of EBF3PanelOpt framework.

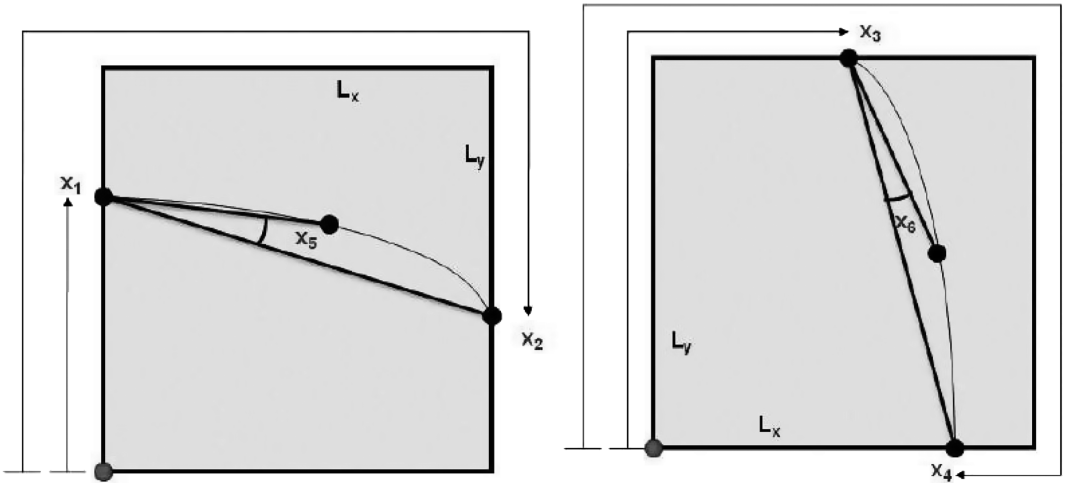

Fig. 2 Design variables identifying the stiffener shape and position.

$$\frac{\sigma_{\text{stiff}}}{F_{\text{cc}}} \leq 1 \tag{3}$$

where σ_{stiff} was taken as the minimum principal stress in the stiffener, and F_{cc} is the maximum allowable stress in the stiffener given by

$$F_{\text{cc}} = \begin{cases} \sigma_y, & 0.61525\left(\frac{b\sqrt{\sigma_y/E}}{t}\right)^{-0.78387} > 1 \\ 0.61525\sigma_y\left(\frac{b\sqrt{\sigma_y/E}}{t}\right)^{-0.78387}, & 0.61525\left(\frac{b\sqrt{\sigma_y/E}}{t}\right)^{-0.78387} \leq 1 \end{cases} \tag{4}$$

where E is the Young's modulus of the stiffener material, b is the stiffener height, and t is the stiffener thickness. The maximum allowable stress formula [Eq. (4)] was obtained from page 444 of [17].

A key ingredient to EBF3PanelOpt is the ability to specify the geometry in a parametric fashion, such that the optimizer fully specifies the panel shape and size by a discrete number of design variables. Size quantities such as panel thickness, stiffener thickness, and stiffener height are used as design variables to define the geometry. The parameterization of the stiffener shape and position merits some clarification. In Fig. 2, the design variables identifying the shape and position of the stiffener are indicated. Note that the beginning and end points of each stiffener are indicated by design variables x_1 to x_4, whereas the shapes of the stiffeners are determined by the angle to the center point (x_5 and x_6). Because rational B-splines are used to determine the stiffener curves, the stiffeners always remain within the panel interior as long as the center point remains in the panel interior.

A total of 11 design variables fully define the panel geometry: variables x_1–x_6 are shown in Fig. 2 and define the stiffener location and shape, variables x_7 and x_8 are the heights of the two stiffeners, variables x_9 and x_{10} are the thicknesses of the stiffeners, and x_{11} is the panel thickness.

III. Combined Loads Test Fixture

To assess the ability of the EBF3PanelOpt for design of panels under complex loading conditions, a combined compression-shear loading condition was selected. The CLTF was developed by researchers at NASA Langley Research Center to perform combined compression-shear load tests on 24 × 28 in. panels [16]. A detailed description of the design, assembly, and operation of the test fixture can be found in [16]. Figure 3 shows the test system without the panel installed. Upper and lower L-shaped shear frames are bolted to the upper and lower compression platens of a 300 kip-capacity compression test system. The lower shear frame is attached to a lateral hydraulic ram to apply the shear loads. The bottom of the lower shear frame rests on roller guides to allow lateral motion. A steel picture frame-type support is attached to the test specimen via a double row of fasteners (see Fig. 4). The picture frame edges are pinned together at the corners to allow in-plane rotation. This support provides the clamped boundary condition to the aluminum panel, while allowing

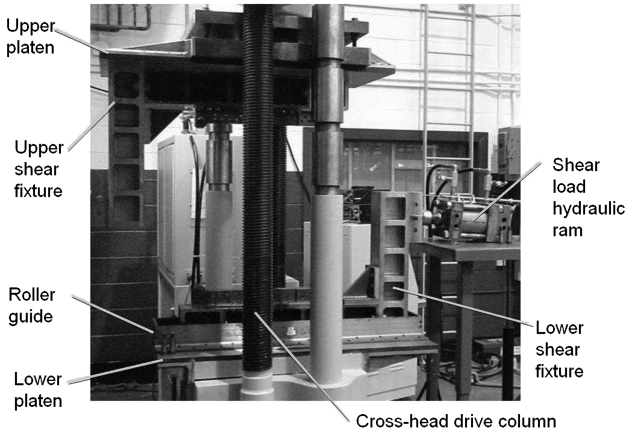

Fig. 3 Compression-shear test system without test panel installed.

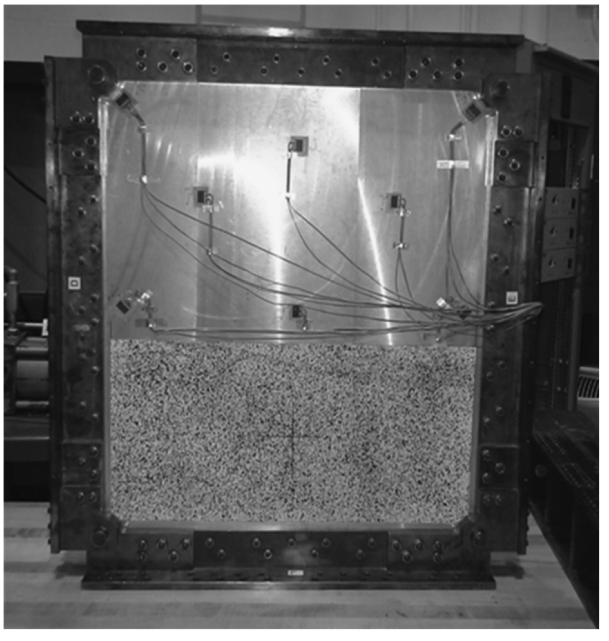

Fig. 4 Picture frame support mounted on a generic test panel.

the panel to deform to a quadrilateral. After installation of the test panel in the CLTF, shear load bars (not shown in Fig. 3) are attached across the upper and lower shear frames to provide a self-reacting shear load mechanism.

IV. Panel Design and Optimization

A 24 × 28 in. curvilinear stiffened panel was designed using the EBF3PanelOpt software and VisualDoc optimization software. The particle swarm optimization (PSO) was used to estimate the global minimum mass, while satisfying constraints on buckling, crippling, and yielding. The VisualDoc optimization parameters for the PSO algorithm used for the analysis are provided in Table 1. For the details regarding the definition of the parameters, please see [18].

The overall panel size was selected based on the capability of the CLTF test system. The panel was designed for a limit load of 42 kips in compression and 9.7 kips in shear (4.35 lb compression per 1 lb shear) against buckling, crippling, and yielding. The material properties of the aluminum alloy used in the panel optimization are shown in Table 2. These properties are for the T76511 condition of Al-7050 from [19]. Table 3 lists the optimal design variables, along with the lower and upper bounds placed on each variable during the optimization.

A. Test Fixture Interface

Early study of the CLTF indicated that it only transmitted about 35% of the compression load into the panel, whereas 100% of the shear load was transmitted to the panel [12]. Therefore, to determine the loading and boundary conditions as closely as possible to those imposed by the CLTF, a reduced grid-point interaction model of the test fixture/panel interface was used within the EBF3PanelOpt framework to apply the loading and boundary conditions during optimization. The reduced model via a superelement was developed from a detailed nonlinear finite element model (FEM) of the fixture developed by Lockheed Martin Aeronautics Co., which may be seen in Fig. 5.

Table 1 VisualDoc optimization parameters for PSO optimization [18]

Parameter	Value
Inertia weight parameter	1.40
Local optimum trust parameter	1.50
Global optimum trust parameter	2.50
Number of particles	20
Maximum number of iterations	70
Minimum number of iterations	5
Absolute objective convergence	10^{-6}
Relative objective convergence	10^{-3}
Absolute design variable convergence	10^{-6}
Relative design variable convergence	10^{-3}

Table 2 Material properties for Al-7050-T76511 used for the panel optimization with EBF3PanelOpt [19]

Parameter	Value
Young's modulus, Msi	10.6
Poisson's ratio	0.33
Yield stress, ksi	68

Table 3 Design variable bounds and optimal values

Design variable	Lower bound	Upper bound	Optimized design
Stiffener 1 starting point, in.	28.4	51.6	43.9
Stiffener 1 ending point, in.	80.4	103.6	89.5
Stiffener 2 starting point, in.	28.4	51.6	37.0
Stiffener 2 ending point, in.	80.4	103.6	95.7
Stiffener 1 angle to midpoint, deg	−10.0	10.0	1.92
Stiffener 2 angle to midpoint, deg	−10.0	10.0	1.95
Height of stiffener 1, in.	0.394	1.969	0.769
Height of stiffener 2, in.	0.394	1.969	0.826
Thickness of stiffener 1, in.	0.039	0.315	0.123
Thickness of stiffener 2, in.	0.039	0.315	0.129
Thickness of the panel, in.	0.039	0.158	0.104

B. Nonlinear Finite Element Model

A nonlinear FEM of the CLTF was developed by Lockheed Martin Aeronautics Co. (see Fig. 5). The FEM includes both elastic-plastic (for the aluminum) and geometric nonlinearity and, thus, is suitable for the postbuckling analysis. The test fixture FE model was developed to interface to a panel model generated by the EBF3PanelOpt. The test fixture was modeled using a total of 44,186 shell, beam, and gap elements. Shell elements were used to model the steel test fixture upper and lower L-arms of the CLTF, as well as the picture frame support secured to the panel (see Fig. 6). The test fixture is constructed predominately from 15-5 (or 17-4) H1025 stainless steel [16]. The material properties used for the test fixture FEM are given in Table 4 [19]. A linear stress-strain relation was used for the test fixture, as the fixture's thickness prevents material nonlinearity therein.

The compressive load is introduced into a single node above the upper L-arm and applied to the upper L-arm using a multipoint constraint (see Fig. 5). The shear load is introduced in a similar manner to the lower L-arm. In each case, two concentric nodes attached by zero-length spring elements were used to provide the appropriate stiffness to the load introduction location. The stiffnesses of these springs were chosen by correlating data from previous Lockheed Martin Aeronautics Co. tests in the CLTF.

Gap elements were used in the FEM to numerically model the "rollers," on which the lower L-arm sits. The gap elements allow the test fixture to pull off the rollers while providing a very large stiffness to prevent penetration. The bottom of the test fixture was constrained to prevent out-of-plane deflection, using two parallel rows of single point constraints applied to the exterior nodes on both sides of the lower L-arm. The shear load was reacted using single point constraints, applied to the bolt locations on the top L-arm (see Fig. 6).

The aluminum test panel was modeled using shell elements. The test panel FEM model was provided by the EBF3PanelOpt analysis software and modified to include the elastic-plastic material model (see Fig. 7). Initial eccentricity of the panel was provided by moving the nodes in the direction of the first buckling mode shape (positive towards the stiffeners) by 0.000104 in., thus producing a slightly imperfect panel to help guide the geometric nonlinear analysis off the trivial solution path. The adhesively bonded steel tabs were modeled using shell elements with an elastic-plastic material law. The stress-strain curve used for the steel tabs is shown in Fig. 7. Zero-length spring elements with stiffness of 41, 250 lb/in. were used to model

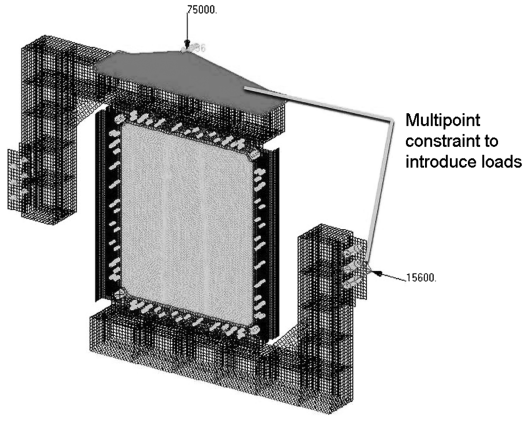

Fig. 5 Detailed FEM of test fixture/curvilinear stiffened panel assembly.

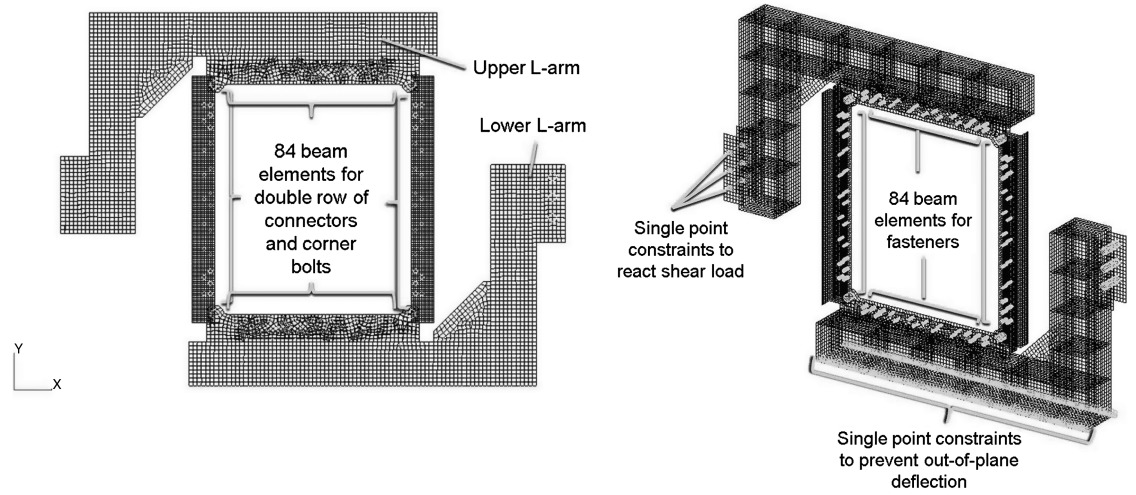

Fig. 6 Steel shell elements in the nonlinear test fixture model and the single point constraints applied to the test fixture model.

Table 4 Material properties used in the nonlinear FEM [19]

Design variable	15-5 (or 17-4) H1025 stainless steel	Al-7050-T851
Young's modulus E, ksi	29,200	10,600
Poisson's ratio ν	0.32	0.33
Yield stress, ksi	152.9	59.4

the adhesive bond. The FEM of the test panel assembly can be seen in Fig. 8.

The double row of fasteners, the four corner fasteners, and the bolts though which the shear load was introduced were modeled using beam elements with appropriate material and geometric properties assigned. The fasteners are shown in Fig. 6.

Initial numerical experiments with the nonlinear test fixture model indicated that the FEM of the test fixture interface used by EBF3PanelOpt incorrectly predicted the buckling load by a substantial amount. The correlated test fixture model was used to extract a grid-point interaction model superelement that would better facilitate the load introduction to the panel in EBF3PanelOpt. Furthermore, the adhesively bonded steel tabs were modeled in the version of EBF3PanelOpt used to design the panel using concentric elements sharing nodes. Whereas the test fixture had geometric spaces between the tabs along the vertical edges, the model in EBF3PanelOpt had no spaces. Therefore, the steel tabs carried much of the load and resulted in a substantially higher predicted buckling load. When the modeling discrepancy was noticed, the panel model/test fixture interface in EBF3PanelOpt was modified to completely remove the steel tabs. The design limit loads of 42 kips compression and 9.7 kips in shear (4.35 lb compression per 1 lb shear) were modified; the new model predicted the onset of buckling at a load of 25 kips in compression and 5.2 kips in shear (4.8 lb compression per 1 lb shear). The test plan was modified to load at the corrected load ratio of 4.8 lb compression per 1 lb shear.

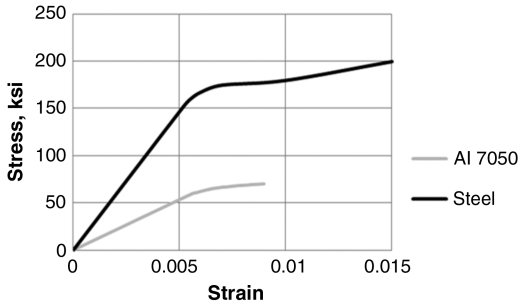

Fig. 7 Elastic-plastic material model for the steel test fixture and the aluminum panel.

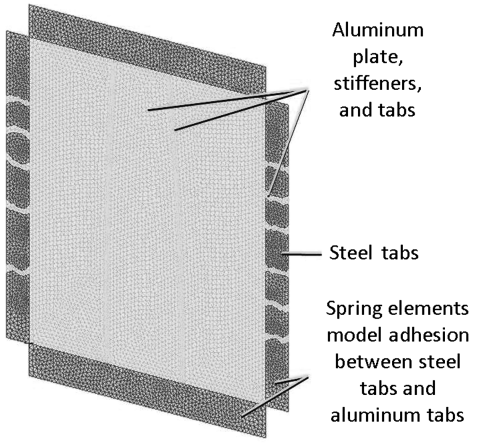

Fig. 8 Model of Al-7050 panel with bonded steel tabs modeled using linear spring elements.

V. Panel Manufacturing

Before manufacturing the baseline optimized panel, a smaller-scale risk reduction panel was constructed that featured variable height curvilinear T-stiffeners (see Fig. 9). This panel was produced to validate the manufacturing process for integrally machined, thin-skinned, stiffened panels. The size of this panel was approximately 16 by 16 in., with 1.5-in.-tall stiffeners at their peak height. Several manufacturability design features were reexamined after coordinating with the machine shop and receiving quotes, including fillet radii and manufacturability stiffness-to-height ratio. The alloy chosen for

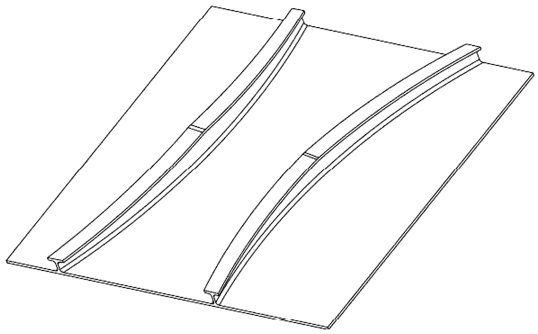

Fig. 9 Risk reduction panel manufactured by Lockheed Martin Aeronautics Co. to verify the integral machining process.

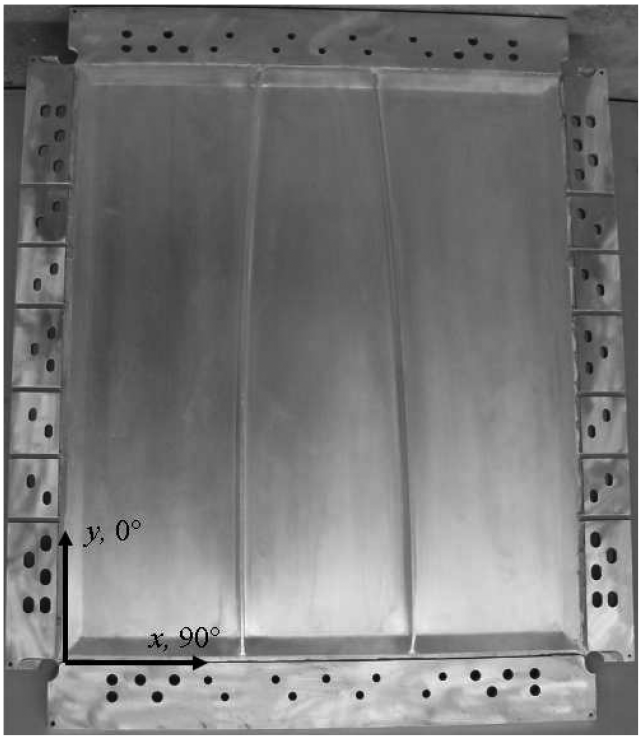

Fig. 10 Picture of the Al-7050 test panel with steel tabs.

the initial manufacturability evaluation and the test panel was 7050 Al heat treated to a T-7451 condition. The material was received as 2-in.-thick plate stock and high-speed machined to the specified risk reduction panel geometry. The completed panel was inspected to ensure that the required tolerances were satisfied and that the panel remained flat on the nonstiffened side. All tolerances were met.

Once the risk reduction panel was completed, the solid model of the baseline curvilinear stiffened panel was converted to a detailed CAD file in CATIA V5 by Lockheed Martin Aeronautics Co. The geometry was modified to include fillets at the panel/stiffener intersections. The test panel used blade stiffeners, as opposed to the T-stiffeners used in the risk reduction panel. The 24×28 in. panel was extended to include 2.94×24 in. tabs along the top and bottom edges, with the bolt pattern specified by the CLTF (see Fig. 10); 2.25×28 in. tabs were also included along the left and right edge of the panel. Whereas the panel had a thickness of 0.104 in., the tabs were required to be 0.25 in. to facilitate the interface between the CLTF and panel. A thickness taper was included to reduce the thickness from 0.25 to 0.104 in. The geometry was also modified to include stiffener runouts at the ends. The CAD file was used to machine the baseline optimized test article from 2-in.-thick plate stock. Postmachining inspection indicated that all required tolerances were met.

After the panel was machined and inspected, 4340 steel tabs conforming to the NASA CLTF drawings [15] were adhesively bonded using Hysol EA9394, with 0.005-in.-diam glass microballoons added for bond-line control. These bonds were cured at room temperature, to prevent any residual thermal expansion stresses at the bond line. The panel was then crated and shipped to NASA Langley Research Center for testing. The completed panel is show in Fig. 10.

VI. Combined Load Compression-Shear Test

A combined load compression-shear test was conducted at NASA Langley Research Center on the panel using the CLTF. Linear variable displacement transducers (LVDTs) were attached to three corners of the top compression platen to measure panel end shortening, and one LVDT was attached to the shear fixture to measure shear displacement.

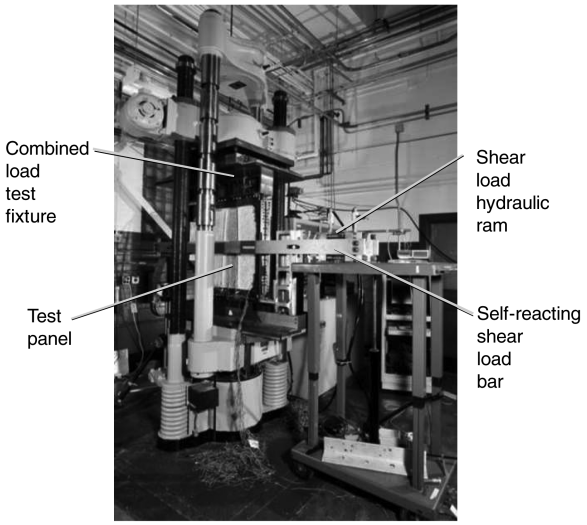

Fig. 11 Compression-shear test system with test panel installed.

A total of 32 strain gages were attached to the panel. Six of the gages were 0/45/90° rosettes, and 26 of the gages were uniaxial gages aligned parallel to the compression load direction. A description of the strain gage locations is provided in Appendix A. The stiffened side of the panel was spray-painted with a speckled pattern to facilitate strain and displacement measurements, using a VIC-3D automated stereophotogrammetic technique. The panel was installed into the CLTF. The lateral shear load hydraulic ram was attached to the CLTF's lower shear frame. The LVDT support brackets and five LVDTs were installed into the test system and attached to the smooth side of the panel, to measure out-of-plane displacement. A description of these LVDT locations is provided in Appendix B.

The data acquisition system was configured to scan and record all of the instrumentation at a rate of one scan per second. The load, displacements, and select strain gages were monitored on a real-time display during the test. The VIC-3D system was configured to obtain full-field stereophotogrammetic displacement/strain measurements on the lower half of the stiffened side of the panel. In addition to the VIC-3D cameras, a video camera was set up to record panel behavior during the test.

Figure 11 shows the test system with the panel installed and ready for testing. Figure 12 shows the stiffened side and flat side of the panel in the test system. The test system was configured to apply compression load and shear load simultaneously, at a compression-shear load ratio of 4.8. A compression load rate of 4000 lb/ min was used. Two preliminary tests were conducted up to a maximum compression load of 5000 lb, to ensure that all of the instrumentation was operational and that the compression-shear load ratio was correct. The data acquisition and VIC-3D systems were started, and compression-shear load application was initiated. The panel was loaded to approximately 60,000 lb in compression, at which point there was a sharp reduction in load and a loud noise. It was assumed that this was a panel structural failure event. The test was stopped, and the load was removed from the panel. Following the load removal, it was discovered that the panel had not been permanently deformed and that the load dropoff and noise events were associated with several of the steel tabs debonding from the panel (see Fig. 13).

VII. Comparison of Experimental and Analytical Results

The test results (LDVTs, strain gages, and out-of-plane displacements from the VIC-3D image correlation system) were compared with results from a nonlinear FEM and the predicted linear response from the FEM, generated by the EBF3PanelOpt script with the revised test fixture/interface model. For all the results, the nondimensional load factor was used to indicate the load level during the proportionally loaded FEM and experiment. The load factor was defined as the ratio of applied load to linear buckling eigenvalue for

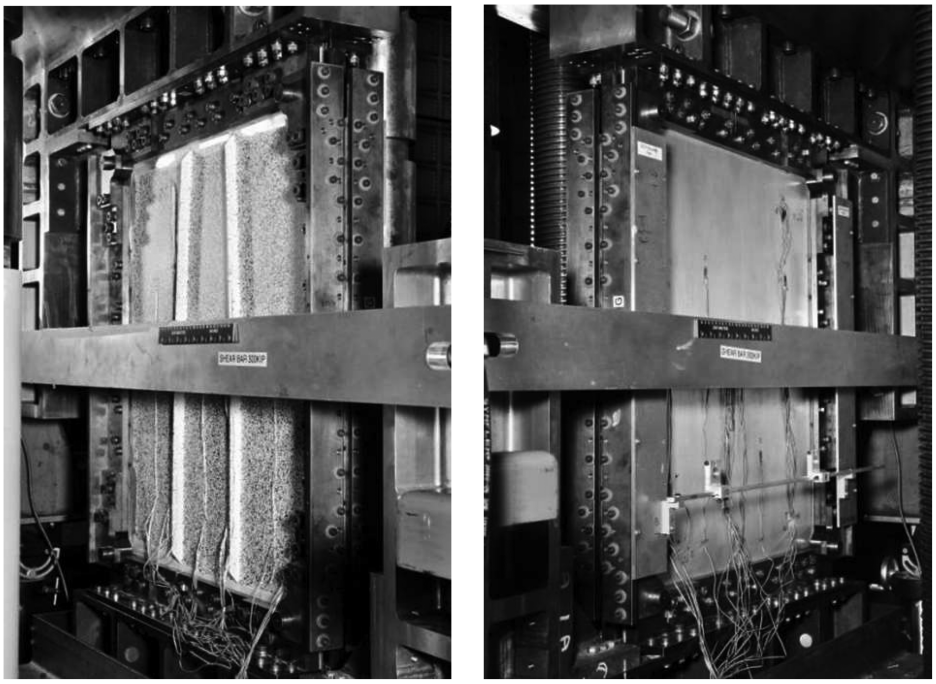

Fig. 12 Stiffened side and flat side of test panel in compression-shear test system.

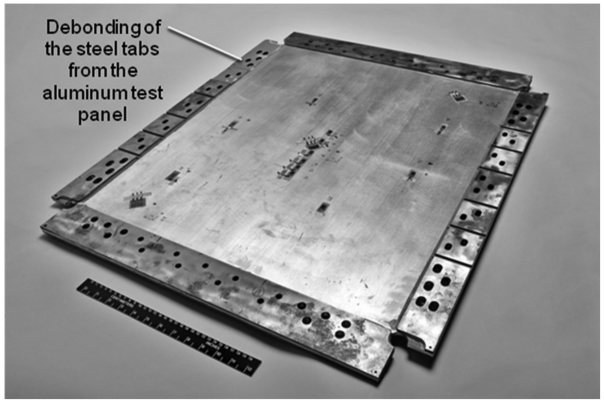

Fig. 13 Posttest photograph of test panel with debonded steel tabs.

the test fixture/panel model. The response of the complete set of 32 strain gages and the 5 LDVT out-of-plane displacement measurements was plotted against the load factor from the nonlinear FEM, linear test fixture/panel assembly model, and the experimental results in [20].

Results obtained by the VIC-3D system were processed and plotted using TecPlot. The contours of measured out-of-plane deflections obtained by the VIC-3D system are compared against the contours of out-of-plane deflection, predicted by the nonlinear FEA in Fig. 14 at a load factor of 1.0 and in Fig. 15 at a load factor of 2.4. The results from the VIC-3D system provided contours over a limited panel surface, with much of the data being removed because it was compromised by the presence of the stiffeners, the stiffener shadows, and strain gage wires. However, the figures indicate that, at a load factor of 1.0, the panel experienced far less out-of-plane deflection than was predicted by the nonlinear FEA. Nonetheless, the contours of deformation appear qualitatively similar in shape to the FEM predictions.

At a load factor of 2.4 (Fig. 15), the contours of out-of-plane deflection obtained by the VIC-3D system compare well qualitatively and quantitatively with the results from the nonlinear FEA. The shape of the contours indicates that the global features of the postbuckled shape compare very well with the analysis. The center deflection of the panel is quantitatively more accurate than at a load factor of 1.0; however, the FEA again predicts higher out-of-plane deflection than that experimentally measured by the VIC-3D.

The measured out-of-plane deflection was plotted against the normalized load factor, in Fig. 16 for LDVT 7 and in Fig. 17 for LDVT 9. The LDVT locations are summarized in Appendix B. The results from the nonlinear FEA and the results from the linear test fixture/panel assembly model are included for comparison. Note that the test results clearly indicate that the panel experiences an initial buckle at a load factor near one, indicated by a dramatic increase in deflection over a small range of load factor. In general, the deflection predicted by FEA is higher than the measured deflection. The deflection predicted by the linear test fixture/panel assembly model compares fairly well within the linear region.

The results from 0° strain gages 5A and 6A are compared in Fig. 18, and the results from 90° strain gages 5B and 6B are compared in Fig. 19. Note that gages 5 and 6 are located just below the center of the panel on the stiffened and flat side of the panel, respectively (see Table A1 and Fig. A1 in Appendix A). Within the linear region, the predicted strain compares very well with that measured by the 0° gages. The response predicted by the linear test fixture/panel assembly model is indistinguishable from the measured strain; however, the postbuckled response of the nonlinear analysis is substantially different from the measured response. The strain on the flat side (gage 6A) of the panel compares very well; however, the FEA predicts substantially greater bending than that seen by the experiment.

Results from the remaining three LDVTs and each of the 32 strain gages were compared against the nonlinear FEA results and the linear test fixture/panel assembly model results in [20]. For the strain gages 5B and 6B, the response is accurately predicted by both the nonlinear FEA and the linear test fixture/panel assembly model within the linear region. The measured response clearly indicates a buckle occurring at a load factor of one. However, there is substantial discrepancy between the postbuckled response predicted by the FEA and measured by the strain gages.

Data from the strain gage rosettes (5 and 6; A, B, and C) were used to obtain the shear strain at gages 5 and 6 by

$$\varepsilon_{xy} = \frac{1}{2}((\varepsilon_{\mathrm{A}} + \varepsilon_{\mathrm{B}}) - 2\varepsilon_{\mathrm{C}}) \tag{5}$$

The experimental shear strain was compared with the predicted responses from the nonlinear and linear FEAs, in Fig. 20. Note that

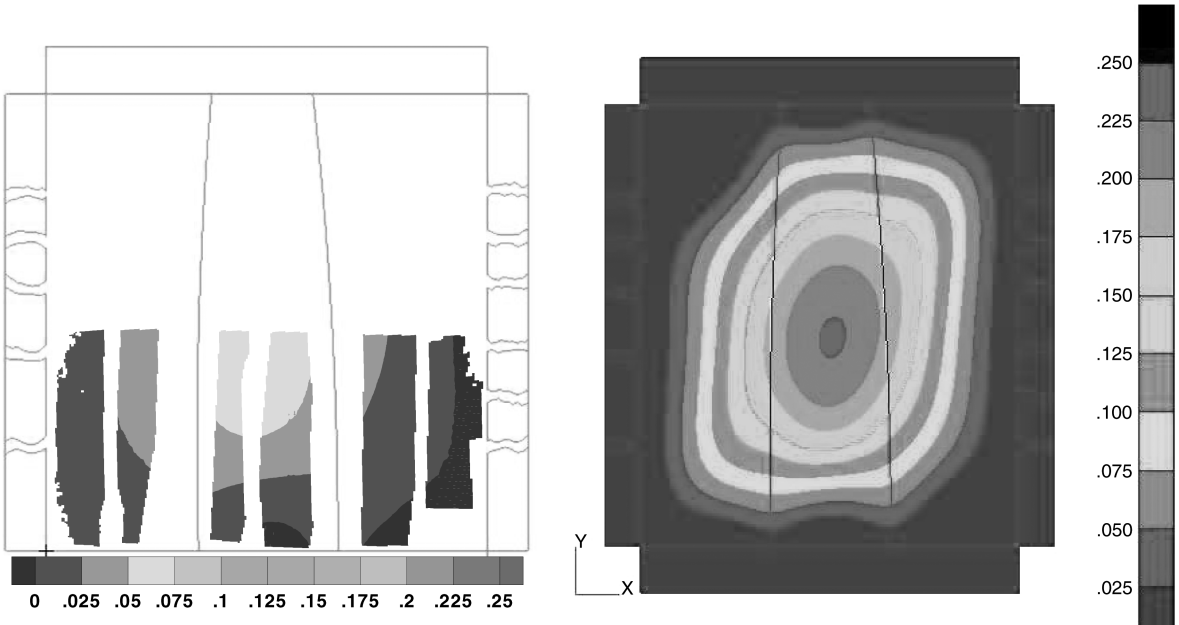

a) Contours of out-of-plane deflection from VIC-3D image correlation system

b) Contours of out-of-plane deflection from the nonlinear finite element model

Fig. 14 Comparison of out-of-plane deflection from VIC-3D image correlation system at a load factor of 1.0: a) contours of out-of-plane deflection from VIC-3D image correlation system and b) contours of out-of-plane deflection from the nonlinear FEM.

there is substantial discrepancy between the predicted and measured response. The predicted strain is almost twice that obtained from the strain gage rosette.

Similar analyses were conducted for strain gage rosettes 21 and 22, located in the bottom right corner of the panel. In Fig. 21, the axial strain was plotted against the normalized load factor from the measured strain gage data, the nonlinear FEA, and the linear test fixture/panel assembly FEA. The figure indicates that the response is accurately predicted by the FEA, even in the postbuckling region.

The shear strain was obtained using the three components of strain from the strain gage rosettes, with Eq. (5). The results were compared against the nonlinear FEA and linear test fixture/panel assembly model that is used by EBF3PanelOpt (see Fig. 22). The figure indicates a much closer correlation between the measured and predicted shear strain than was seen for gages 5 and 6. In the linear region, the linear model accurately predicts the shear strain. For the flat side of the panel (strain gage 22), the nonlinear FEA and the test response are nearly indistinguishable. However, for the stiffened side of the panel (strain gage 21), the measured response is substantially different from the predicted response in the postbuckling region.

The discrepancies between the measured and predicted deflection and strains are most likely the result of modeling inaccuracies in the FE models. It should be noted that the taper between the 0.25-in.-thick aluminum tabs and the 0.103-in.-thick panel (see Fig. 10) was

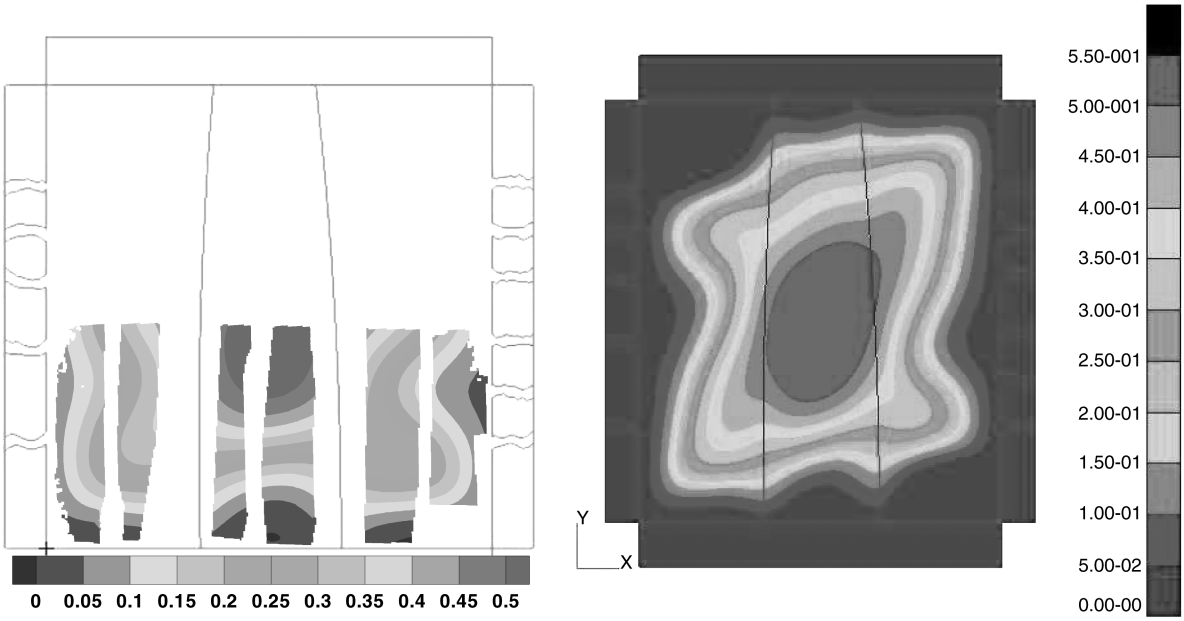

a) Contours of out-of-plane deflection from VIC-3D image correlation system

b) Contours of out-of-plane deflection from the nonlinear finite element model

Fig. 15 Comparison of out-of-plane deflection from VIC-3D image correlation system at a load factor of 2.4: a) contours of out-of-plane deflection from VIC-3D image correlation system and b) contours of out-of-plane deflection from the nonlinear FEM.

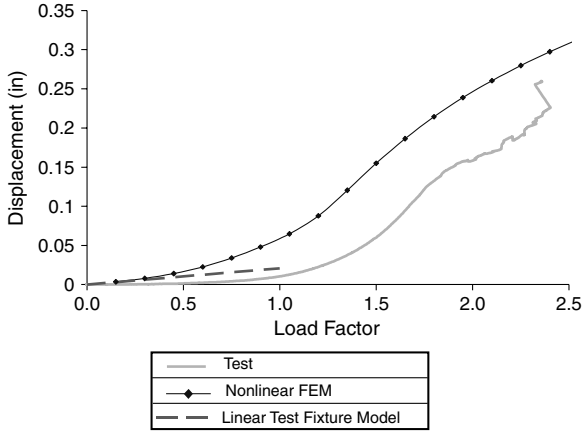

Fig. 16 Comparison of the test, nonlinear FE model, and the linear test fixture/panel assembly model responses for LVDT 7 (positive deflection is measured towards the stiffeners).

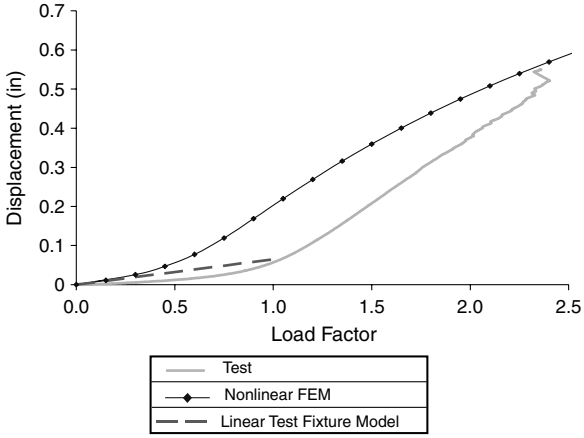

Fig. 17 Comparison of the test, nonlinear FE model, and the linear test fixture/panel assembly model responses for LVDT 9 (positive deflection is measured towards the stiffeners).

modeled as a sudden change in thickness between plates whose midsurfaces were aligned. The effect of the misalignment between the midsurfaces of the 0.25 in. tabs and the 0.103 in. panel would result in a moment that would reduce the out-of-plane deflection in the buckled response. Furthermore, the strains on the flat side of the panel tracked closer with the experimental results than the stiffened side. The effect of the moment would reduce the amount of bending and could potentially account for the discrepancies of the strains on the stiffened side of the panel. Future FE models of tests in the CLTF should model very closely the load introduction mechanism (taper), to prevent such discrepancies.

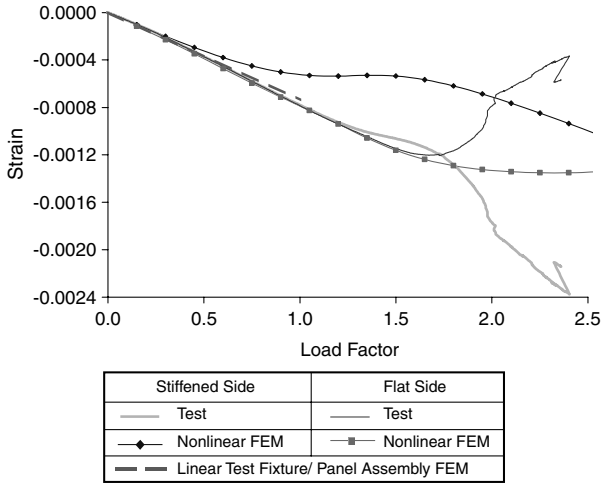

Fig. 18 Comparison of the test, nonlinear FEA, and the linear test fixture/panel assembly responses for axial strain gages 5A and 6A (ε_{yy}).

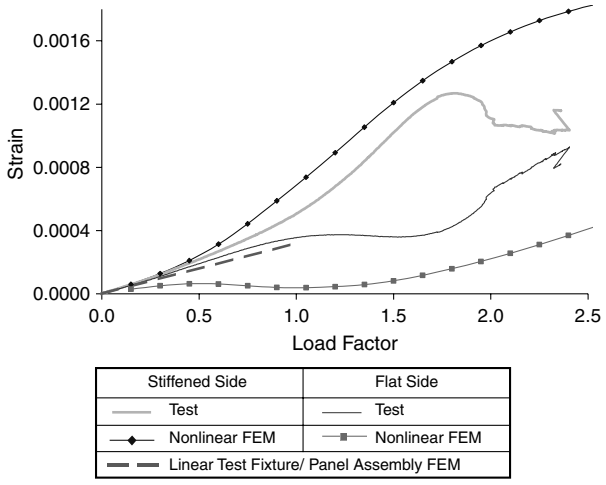

Fig. 19 Comparison of the test, nonlinear FEA, and the linear test fixture/panel assembly responses for strain gages 5B and 6B oriented perpendicular to the direction of the dominant compressive loading (ε_{xx}).

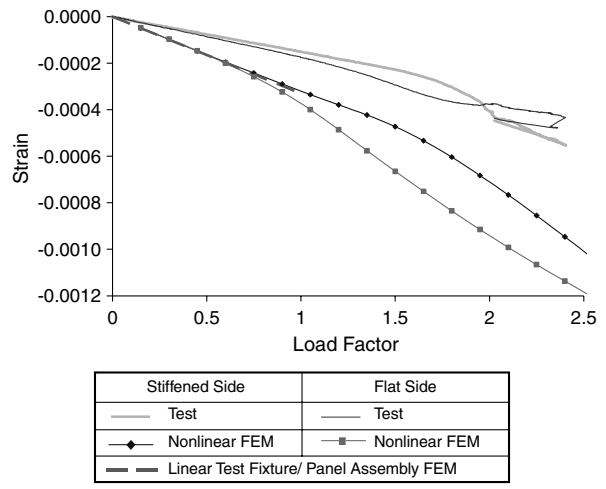

Fig. 20 Comparison of the test, nonlinear FEA, and the linear test fixture/panel assembly responses for shear strain extracted from strain gages rosettes 5 and 6 (ε_{xy}).

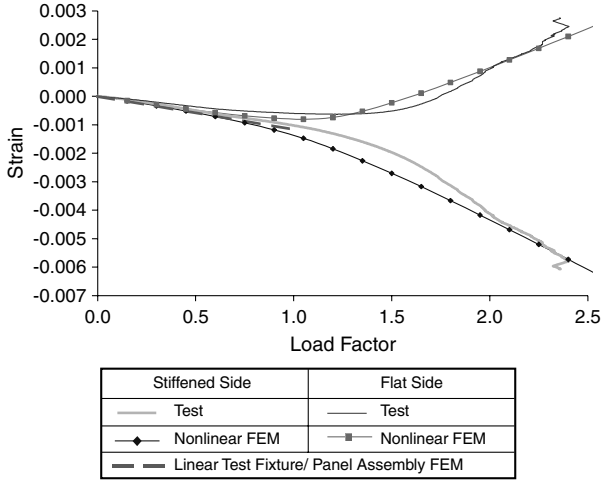

Fig. 21 Comparison of the test, nonlinear FEA, and the linear test fixture/panel assembly responses for axial strain gages 21A and 22A (ε_{yy}).

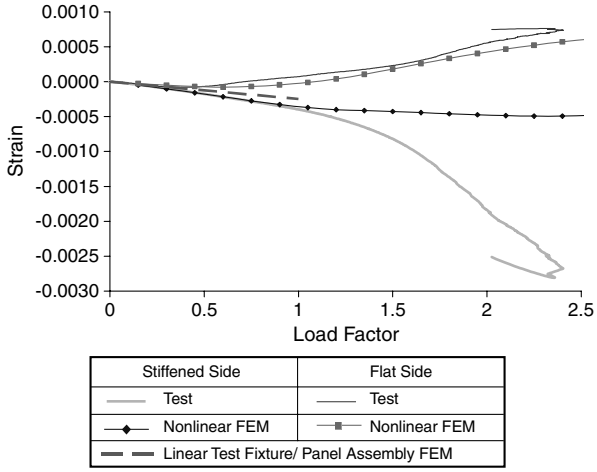

Fig. 22 Comparison of the test, nonlinear FEA, and the linear test fixture/panel assembly responses for shear strain extracted from strain gages rosettes 21 and 22 (ε_{xy}).

VIII. Conclusions

A new analysis tool, EBF3PanelOpt, is being developed for design and optimization of complex multifunctional aircraft structural concepts. The tool was used to design and optimize a baseline structural panel with curved stiffeners. The panel was optimized for minimum mass subjected to constraints on buckling load, yielding, and crippling or local stiffener failure. The panel was designed for a combined compression-shear loading configuration that is a realistic load case for a typical aircraft wing panel. The optimized panel design was used to fabricate an integrally machined test panel, using aluminum alloy 7075-T851. The panel was tested at NASA Langley Research Center in the combined load test fixture under combined compression-shear loading. The test results were compared against analytical results obtained using MSC.Nastran. Both a linear FEA, which was generated by EBF3PanelOpt, and a detailed nonlinear FEA were compared with the test results in an attempt to verify the accuracy of assumptions and modeling techniques used by the EBF3PanelOpt software.

From the comparison of the numerical test results and the FEA, the following observations were made:

1) The panel buckled at the predicted linear buckling eigenvalue. Pretest modifications to test fixture FE modeling, which interfaces with EBF3PanelOpt, corrected the linear buckling eigenvalue.

2) Before buckling, the strains and deflections are reasonably accurately predicted by EBF3PanelOpt, with the exception of the shear strain at the center of the panel. The shear strain in this region was overpredicted by a factor of two.

3) The out-of-plane deflection measured by the VIC-3D image correlation system indicates a good qualitative comparison between the FEA and the test results; however, the panel experienced

Table A1 Location of strain gages on baseline compression-shear test panel

Gage number	Gage type	Orientation, deg	x, in.	y, in.	Location	Figure
1	Uniaxial	0	0	1.58	Skin on stiffened side of panel	A1
2	Uniaxial	0	0	1.58	Skin on flat side of panel	A1
3	Uniaxial	0	0	0.22	Skin on stiffened side of panel	A1
4	Uniaxial	0	0	0.22	Skin on flat side of panel	A1
5A	Rosette	0	0	−0.68	Skin on stiffened side of panel	A2
5B	Rosette	90	0	−0.68	Skin on stiffened side of panel	A2
5C	Rosette	45	0	−0.68	Skin on stiffened side of panel	A2
6A	Rosette	0	0	−0.68	Skin on flat side of panel	A2
6B	Rosette	90	0	−0.68	Skin on flat side of panel	A2
6C	Rosette	45	0	−0.68	Skin on flat side of panel	A2
7	Uniaxial	0	0	−1.51	Skin on stiffened side of panel	A2
8	Uniaxial	0	0	−1.51	Skin on flat side of panel	A2
9	Uniaxial	0	0	−2.71	Skin on stiffened side of panel	A2
10	Uniaxial	0	0	−2.71	Skin on flat side of panel	A2
11	Uniaxial	0	0	−3.53	Skin on stiffened side of panel	A2
12	Uniaxial	0	0	−3.53	Skin on flat side of panel	A2
13	Uniaxial	0	0	−4.35	Skin on stiffened side of panel	A2
14	Uniaxial	0	0	−4.35	Skin on flat side of panel	A2
15	Uniaxial	0	−7.88	−0.68	Skin on stiffened side of panel	A2
16	Uniaxial	0	−7.88	−0.68	Skin on flat side of panel	A2
17	Uniaxial	0	7.88	−0.68	Skin on stiffened side of panel	A2
18	Uniaxial	0	7.88	−0.68	Skin on flat side of panel	A2
19	Uniaxial	0	7.88	−8.40	Skin on stiffened side of panel	A2
20	Uniaxial	0	7.88	−8.40	Skin on flat side of panel	A2
21A	Rosette	0	7.88	−11.98	Skin on stiffened side of panel	A2
21B	Rosette	90	7.88	−11.98	Skin on stiffened side of panel	A2
21C	Rosette	45	7.88	−11.98	Skin on stiffened side of panel	A2
22A	Rosette	0	7.88	−11.98	Skin on flat side of panel	A2
22B	Rosette	90	7.88	−11.98	Skin on flat side of panel	A2
22C	Rosette	45	7.88	−11.98	Skin on flat side of panel	A2
23A	Rosette	0	−7.88	10.82	Skin on stiffened side of panel	A1
23B	Rosette	90	−7.88	10.82	Skin on stiffened side of panel	A1
23C	Rosette	45	−7.88	10.82	Skin on stiffened side of panel	A1
24A	Rosette	0	−7.88	10.82	Skin on flat side of panel	A1
24B	Rosette	90	−7.88	10.82	Skin on flat side of panel	A1
24C	Rosette	45	−7.88	10.82	Skin on flat side of panel	A1
25	Uniaxial	0	−7.88	5.95	Skin on stiffened side of panel	A1
26	Uniaxial	0	−7.88	5.95	Skin on flat side of panel	A1
27	Uniaxial	0	——	−6.70	Stiffener A	A3
28	Uniaxial	0	——	−6.70	Stiffener A	A3
29	Uniaxial	0	——	−6.70	Skin on flat side of panel directly behind stiffener A	A3
30	Uniaxial	0	——	5.52	Stiffener B	A4
31	Uniaxial	0	——	5.52	Stiffener B	A4
32	Uniaxial	0	——	5.52	Skin on flat side of panel directly behind stiffener B	A4

substantially less out-of-plane deflection than was predicted by the nonlinear FEA.

4) Comparison of the postbuckled response with the nonlinear FEM indicated that there are substantial discrepancies. Gages located in the corners of the panel showed very accurate postbuckling predictions by the FEA, whereas the predictions for gages along the centerline of the panel were substantially erroneous.

It should be noted that it is not surprising that the postbuckling response is not predicted well by the analysis. The postbuckling response depends heavily on synergistic effects of modeling inaccuracies. Within the nonlinear FEM, springs are used to introduce the load into the panel. The stiffness of these springs has been tuned and correlated to previous test data.

The accuracy of the predicted response before buckling is a substantial accomplishment and indicates that the information used by EBF3PanelOpt to predict the buckling, von Mises, and crippling constraints are accurate. Furthermore, this study has shown that it is critical to allow the user to correctly apply the loading and boundary conditions when using EBF3PanelOpt. For the current design, a superelement representing the test fixture was used to constrain the panel and apply the loading. This approach is limited to the test fixture and would require substantial changes to the EBF3PanelOpt script. EBF3PanelOpt currently also allows for uniform loading and uniform clamped or free edge boundary conditions. Although this covers a variety of loading configurations, it is not generic. It is recommended that EBF3PanelOpt provide the most generality in applying the boundary conditions and loading.

Appendix A: Strain Gage Locations

A total of 32 strain gages were attached to the baseline compression-shear curvilinear stiffened test panel. Six of the strain gages were type CEA13-250UR-350 rosettes (0/45/90°), with 0° direction oriented parallel to the compression load direction. Three of these rosettes were attached to the skin on the stiffened side of the panel, and three were attached to the skin on the flat side of the panel. The other 26 gages were type CEA00-250UW-350 uniaxial gages,

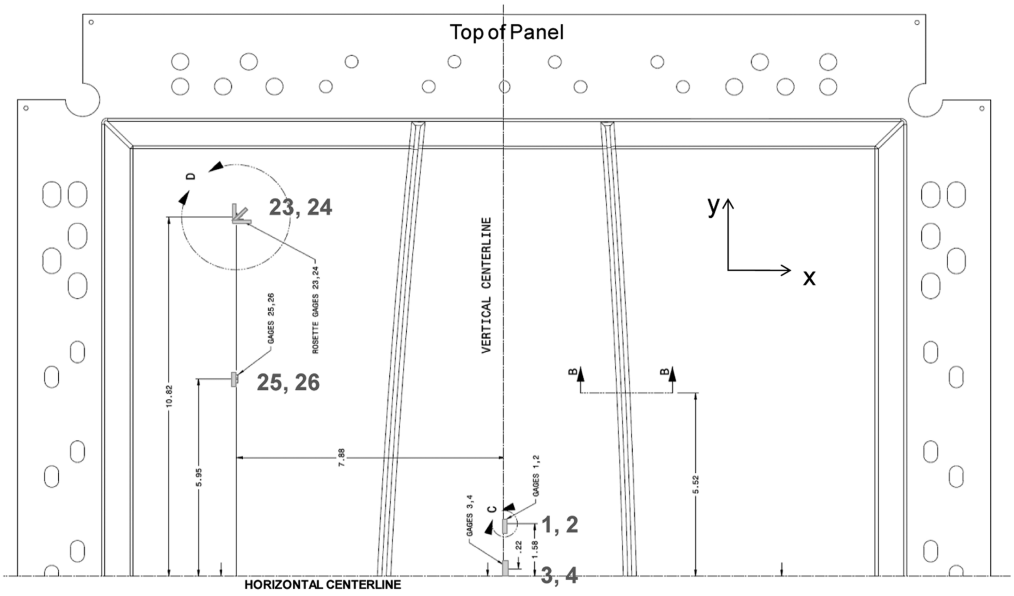

Fig. A1 Location of strain gages on top half of test panel.

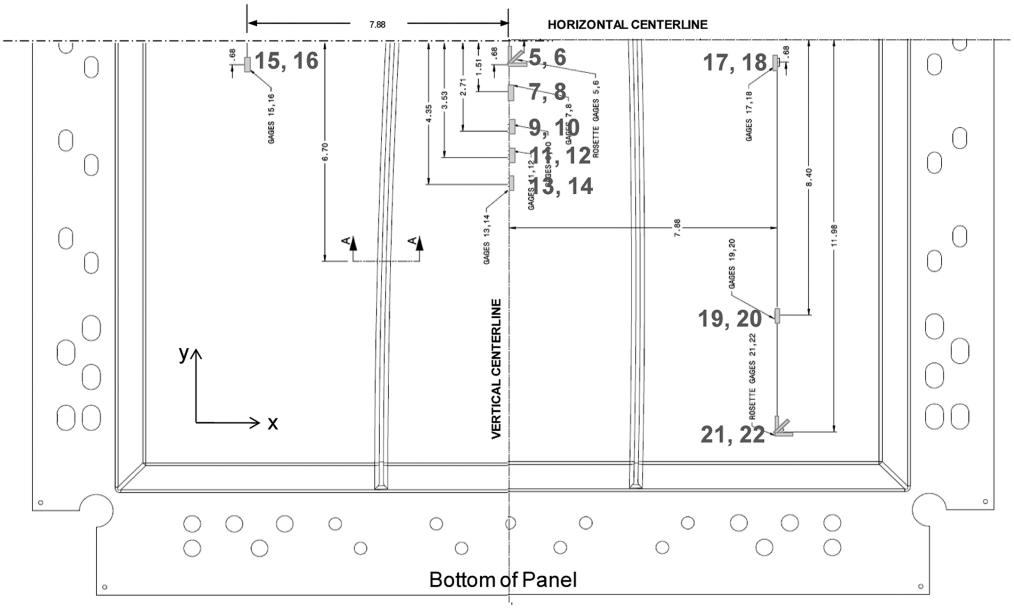

Fig. A2 Location of strain gages on bottom half of test panel.

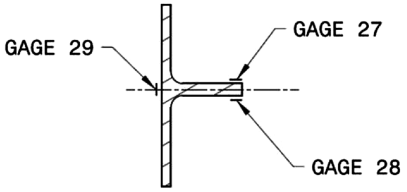

Fig. A3 Location of strain gages on stiffener A.

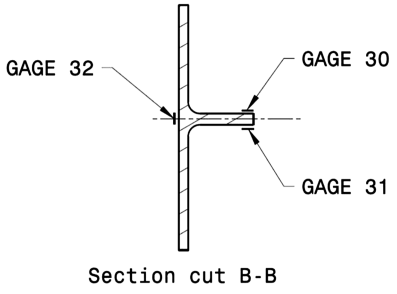

Fig. A4 Location of strain gages on stiffener B.

oriented parallel to the compression load direction. Ten of these uniaxial gages were attached to the skin on the stiffened side of the panel, and ten were attached to the skin on the flat side of the panel. Four of the uniaxial gages were attached to the stiffeners. The remaining two uniaxial gages were attached to the skin on the flat side of the panel, directly behind the two stiffeners.

Table A1 shows an itemized list of the strain gages and their locations on the panel. Figure A1 shows the strain gage locations on the top half of the panel, and Fig. A2 shows the strain gage locations on the bottom half of the panel. The intersection of the vertical and horizontal centerlines is considered to be the zero position point on the panel. When viewing the stiffened side of the panel, the positive horizontal direction x is moving to the right. The positive vertical direction y is moving upward. The left-hand stiffener is stiffener A, and the right-hand stiffener is stiffener B. Figures A3 and A4 show the strain gage locations attached to stiffeners A and B, respectively.

Appendix B: Location of Linear Variable Displacement Transducers for Out-of-Plane Displacement Measurement

A total of five LVDTs were attached to the baseline compression-shear curvilinear stiffened test panel. The LVDTs were attached to the smooth side of the panel using mounting brackets attached to the test machine. The LVDTs were configured such that an outward buckling of the smooth side of the panel would result in a positive displacement reading on the data acquisition system.

Table B1 shows an itemized list of the LVDTs and their locations on the panel. Figure B1 shows the LVDT locations. All of the LVDTs were positioned on the bottom half of the test panel. The intersection of the vertical and horizontal centerlines is considered to be the zero position point on the panel. When viewing the stiffened side of the panel, the positive horizontal direction x is moving to the right. The positive vertical direction y is moving upward. The left-hand stiffener is stiffener A, and the right-hand stiffener is stiffener B.

Table B1 Location of LVDTs on baseline compression-shear test panel

LVDT number	x, in.	y, in.
4	−8.0	−2.7
5	6.9	−12.2
6	7.4	−6.9
7	8.5	−2.7
9	−1.0	−2.7

Acknowledgments

The work presented here was funded under NASA subsonic fixed wing hybrid body technologies NASA research announcement (NRA) NASA NN L08AA02C, with Karen M. Brown Taminger as the associate principal investigator and Cynthia Lach as the contract monitor. We are thankful to both Taminger and Lach for their suggestions. The authors would like to thank our partners in the NRA project, John Barnes and Steve Englestad, of Lockheed Martin Aeronautics Co. of Marietta, Georgia, for technical discussions. Compression-shear tests were conducted at NASA Langley Research Center, under the subsonic fixed wing program.

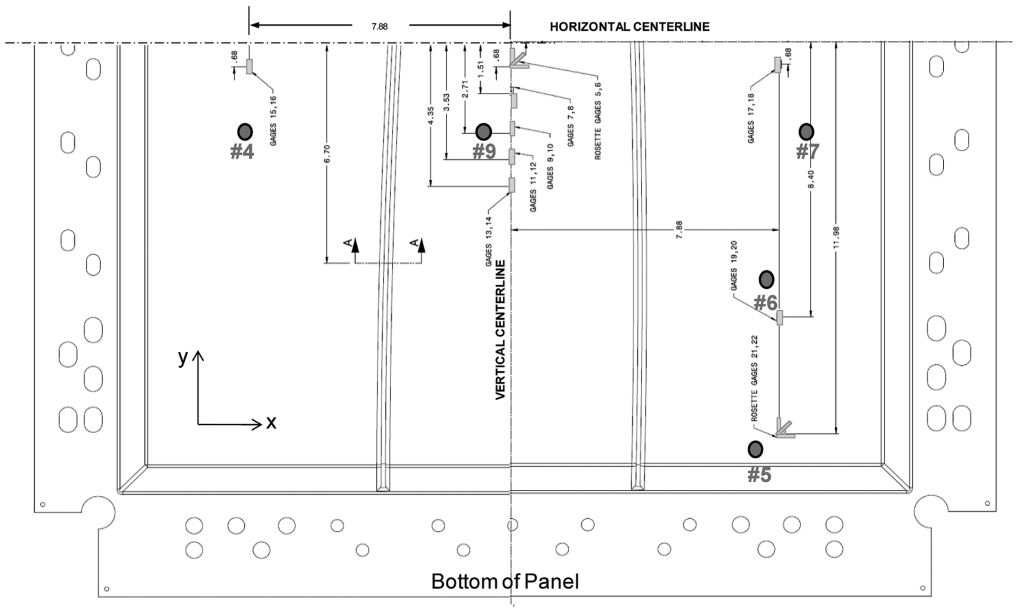

Fig. B1 Location of LVDTs on test panel.

References

[1] Bendsoe, M., and Kikuchi, N., "Generating Optimal Topologies in Optimal Design Using a Homogenization Method," *Computer Methods in Applied Mechanics and Engineering*, Vol. 71, No. 2, 1988, pp. 197–224.
doi:10.1016/0045-7825(88)90086-2

[2] Schramm, U., and Zhou, M., "Recent Developments in the Commercial Implementation of Topology Optimization," *IUTAM Symposium on Topological Design Optimization of Structures, Machines and Materials: Solid Mechanics and its Applications*, Vol. 137, Part 6, 2006, pp. 239–248.

[3] Bendsoe, M., and Sigmund, O., *Topology Optimization: Theory, Methods, and Applications*, Springer–Verlag, Berlin, 2003, p. 11.

[4] Schramm, U., Zhou, M., Tang, P., and Harte, C., "Topology Layout of Structural Designs and Buckling," 10th AIAA/ISSMO Multidisciplinary Analysis and Optimization Conference, AIAA Paper 2004-4636, Albany, NY, 30 July–1 Aug. 2004.

[5] Bushnell, D., "PANDA2: Program for Minimum Weight Design of Stiffened, Composite, Locally Buckled Panels," *Computers and Structures* Vol. 25, No. 4, 1987, pp. 469–605.
doi:10.1016/0045-7949(87)90267-7

[6] Akl, W., El-Sabbagh, A., and Baz, A., "Optimization of the Static and Dynamic Characteristics of Plates with Isogrid Stiffeners," *Finite Elements in Analysis and Design*, Vol. 44, No. 8, May 2008, pp 513–523.
doi:10.1016/j.finel.2008.01.015

[7] Nicholas, E., "Developments in the Friction-Stir Welding of Metals," *ICAA-6: 6th International Conference on Aluminum Alloys*, 1998.

[8] Taminger, K., Hafley, R., and Dicus, D., "Solid Freeform Fabrication: An Enabling Technology for Future Space Missions," *Keynote Lecture for 2002 International Conference on Metal Powder Deposition for Rapid Manufacturing Metal Powder Industries Federation*, San Antonio, TX, 8–10 April 2002, pp. 51–56.

[9] Chan, K., Harter, J., Grandt, A., and Honeycutt, K., "Enhanced Crack Growth Methodology and Analyses for Unitized Structures," *Ninth Joint FAA/DoD/NASA Conference on Aging Aircraft*, Atlanta, GA, 6–9 March 2006.

[10] Renton, W., Olcott, D., Roeseler, W., Batzer, R., Baron, W., and Velicki, A., "Future of Flight Vehicle Structures (2000–2023)," *Journal of Aircraft*, Vol. 41, No. 5, 2004, pp. 986–997.
doi:10.2514/1.4039

[11] Pettit, R., Wang, J., and Toh, C., "Validated Feasibility Study of Integrally Stiffened Metallic Fuselage Panels for Reducing Manufacturing Costs," NASA CR-2000-209342, Boeing, Long Beach, CA, 2000.

[12] Gurav, S., and Kapania, R., "Development of Framework for the Design Optimization of Unitized Structures," 50th AIAA/ASME/ASCE/AHS/ASC Structures, Structural Dynamics, and Materials Conference, AIAA Paper 2009-2186, Palm Springs, CA, 4–7 May 2009.

[13] Mulani, S., Joshi, P., Li, J., Kapania, R., and Shin, Y., "Optimal Design of Unitized Structures with Straight/Curvilinear Stiffeners Using Response Surface Approaches," *Journal of Aircraft*, Vol. 47, No. 6, Nov.–Dec. 2010, pp. 1898–1906.
doi:10.2514/1.47411

[14] Joshi, P., Mulani, S., Gurav, S., and Kapania, R., "Design Optimization for Minimum Sound Radiation from Point-Excited Curvilinearly Stiffened Panel," 50th AIAA/ASME/ASCE/AHS/ASC Structures, Structural Dynamics, and Materials Conference, AIAA Paper 2009-2649, Palm Springs, CA, 4–7 May 2009.

[15] Dang, T., Kapania, R., and Gurav, S., "Optimization of Unitized Structures Under Damage Tolerance Constraints," 50th AIAA/ASME/ASCE/AHS/ASC Structures, Structural Dynamics, and Materials Conference, AIAA Paper 2009-2550, Palm Springs, CA, 4–7 May 2009.

[16] Baker, D., "Combined Load Test Fixture," NASA TM-2010-216211, March 2010.

[17] Niu, M. (ed.), *Airframe Stress Analysis and Sizing*.2nd ed., Conmilit, Hong Kong, 1997, p. 444.

[18] Venter, G., and Sobieszczanski-Sobieski, J., "Particle Swarm Optimization," 43rd AIAA/ASME/ASCE/AHS/ASC Structures, Structural Dynamics, and Materials Conference, AIAA Paper 2002-1235, Denver, CO, 22–25 April 2002.

[19] "Metallic Materials and Elements for Aerospace Vehicle Structures," *Department of Defense Handbook*, U.S. Dept. of Defense, Washington, D.C., 31 Jan. 2003.

[20] Slemp, W., Bird, R., Kapania, R., Havens, D., Norris, A., and Olliffe, R., "Design, Optimization, and Evaluation of Integrally-Stiffened Al-7050 Panel with Curved Stiffeners," NASA TR (to be published).